Application of layered Nickel/Indium double hydroxide in the highly efficient removal of crystal violet dye from textile effluent

Eduardo Teixeira Santos[1], Nicholas P. Power[2], Satheesh Krishnamurthy[3,4], Daniel A. Bertuol[1], Eduardo H. Tanabe[1*]

[1] *Environmental Processes Laboratory (LAPAM), Chemical Engineering Department, Federal University of Santa Maria – UFSM, Santa Maria, RS, Brazil*

[2] *School of Life, Health & Chemical Sciences, The Open University, Milton Keynes, MK7 6AA, United Kingdom.*

[3] *School of Engineering & Innovation, The Open University, Walton Hall, Milton Keynes MK7 6AA, UK*

[4] *Surrey Ion Beam Centre, Advanced Technology Institute, University of Surrey, Guildford Surrey GU2 7XH, United Kingdom*

Abstract

Worldwide freshwater demand will soon exceed supply if measures are not taken to mitigate inadequate wastewater treatment and its indiscriminate release into the environment. The textile industry is one of the largest consumers of freshwater and the third largest contributor to clean water pollution. Conventional treatment of textile effluent is inadequate and expensive. Adsorbent materials obtained from discarded solid waste precursors that contain high amounts of valuable metals can be an inexpensive way to obtain a highly efficient and low-cost wastewater treatment process. This study developed and explored a highly efficient adsorbent layered double hydroxide of Nickel and Indium (Ni/In-LDH) for the adsorption of widely used textile cationic dye, crystal violet (CV). The adsorbent material was synthesized by co-precipitation process of indium nitrate and nickel nitrate. The adsorbent material morphology and its adsorption capacity were investigated in different studies, such as the influence of pH, dosage,

kinetics, isotherms, thermodynamics, ionic strength, adsorbent regeneration capacity, and interaction mechanisms of adsorption. Optimal operating conditions for Ni/In-LDH adsorption revealed maximum adsorption capacity Q_{max} of 570.94 mg g^{-1} at starting pH 8 and 60°C, which maintained approximately 75% of the initial adsorption capacity in three successive adsorption/regeneration cycles. The experimental data fitted Pseudo first order kinetic model (PFO) and the Liu isothermal adsorption model. Thermodynamic studies indicated a spontaneous endothermic adsorption process, and a mechanism of physisorption of CV onto Ni/In-LDH substrate. After FTIR analysis of CV loaded Ni-In/LDH, electrostatic, hydrogen bonding, and n-π bonding interactions were suggested as the interaction mechanisms of adsorption. The Ni/In-LDH demonstrated excellent performance in the removal of CV dye in aqueous solutions compared to other high performing adsorbents.

Keywords: Adsorption; effluent treatment; cationic dye; anionic clay; textile wastewater.

*Corresponding author: edutanabe@ufsm.br

Environmental Processes Laboratory (LAPAM), Chemical Engineering Department, Federal University of Santa Maria – UFSM, Av. Roraima 1000, 97105–900 Santa Maria, RS, Brazil.

1. Introduction

With continued industrial expansion and ever-increasing demand on natural resources, past and current industrial practices are unsustainable for their impact on water globally. Currently 2 billion people (25% of world's population) lack safe drinking water and 1.4 billion people suffer from water scarcity, with current predictions of freshwater demand exceeding supply by 40% by 2030 [1]. Globally, the textile industry is significant in its consumption of fresh water (reaching 100 billion m^3 per year by 2025) and is one of the largest contributors to clean water pollution by dyes. Approximately 30% of wastewater is produced by industries [2]. The management of textile industry effluent is imperative to prevent the toxic, teratogenic, carcinogenic and xenobiotic consequences of contact with contaminants present in dye wastewater to human health and the environment [3]. Dyes are resistant to aerobic digestion, stable under exposure to light, heat, and oxidizing agents. They can be classified based on their solubility in water, chemical structure, applications, and ionic nature [3,4]. Cationic dyes form-colored cationic salts in aqueous solutions, with functional groups such as acid-soluble amino and substituted amino compounds ($-NR^{3+}$ or $=NR^{2+}$) that bind via ionic bonds with the anionic groups of the textile fiber [4,5]. Among the industrial dyes, Crystal violet (Tris(4-(dimethylamino)phenyl)-methylium chloride, (CV)) stands out, oft referred to as triphenylmethane dyes, they are highly soluble in ethanol but have lower solubility in water. The vibrant purple color of CV is due high stability of the carbocation. This stability is responsible for the recalcitrance of CV and results from the delocalized positive charge of the central carbon by the resonance mechanism of the three nitrogen (Fig. 1), and the delocalization of charge across the double bonds in the benzene rings [6].

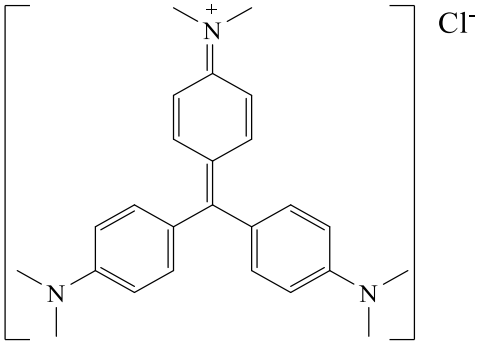

Fig. 1 – Crystal violet molecular structure.

To improve drinkable water access, it is necessary to reduce costs in wastewater treatment and the incorrect wastewater management, developing and exploring new effluent treatment processes that are easier and cheaper to install and operate worldwide in industrial scale. The adsorption process is the most employed of the physicochemical methods of wastewater treatment, where the effluent is mixed or percolates the porous surface of the material in powder or granules of the adsorbent, such as activated carbon or clays [7,8]. Some advantages of adsorption processes are A) the possibility of regenerating the adsorbent, B) the high efficiency for a wide variety of dyes, C) the flexibility of the process, and D) the low operating costs of the process [3,8].

The adsorbent most used for this purpose is activated carbon, which has great selectivity for reactive, basic, and azo dyes. However, activated carbon cannot be reused afterwards, is not able to adsorb suspended solids and insoluble dyes, and carries a high cost for regeneration [3,7,9]. To solve some of these drawbacks, researchers are investigating new adsorbent materials based on LDH, also known as anionic clays, an important class of ionic layered solids, with a general formula $[M^{2+}_{(1-x)}M^{3+}_{x}(OH)_2]^{x+}(A^{n-})_{x/n}.YH_2O$, widely used in ion exchanges, catalysis, or as a support for catalysts and adsorbents [10]. Several LDH materials have been used in CV adsorption, such as Zn-Al LDH [11], Mg-AL/LDH [12] and CaAl/LDH [13]. A synthesis

of LDH from nickel nitrate and indium nitrate was described by Wang *et al*. [14], obtaining the adsorbent material Ni/In-LDH intercalated with carbonate (CO_3^{2-}), being used in DNA adsorption. However, to the best of our knowledge, the use of Ni/In-LDH in dye adsorption processes has not been reported in the literature. Metals recovered from Waste Electrical and Electronic Equipment (WEEE) when applied as precursor materials in the production of effective adsorbents can further reduce costs for treating effluents from the textile industry. Studies already recovered materials such as nickel from spent batteries [15] and indium obtained from LCD screens of discarded cellphones [16].

Herein, exploration and development of an efficient adsorbent composed of Ni/In-LDH for the removal of Crystal Violet dye in aqueous solutions was pursued as the main objective of this work. Characterization of the adsorbent material was performed to investigate the morphology and the adsorption process mechanisms of the adsorbent material. The effects of *pH* and *pH* at the point of zero charge (pH_{pzc}), adsorbent dosage, kinetics, isotherms, thermodynamics, ionic strength, and adsorbent regeneration capacity were investigated in the adsorption experiments, and interaction mechanisms of adsorption were proposed.

2. Experimental methodology

2.1. Materials

Reagents for the synthesis of LDH: Sodium hydroxide (purity 98.0%, Dinâmica Química Contemporânea LTDA/Brazil), Nickel (II) nitrate hexahydrate (purity 97.0%, Neon Reagentes Analíticos/Brazil), Indium nitrate (III) pentahydrate (purity 99.9%, Sigma-Aldrich Co Ltd./Brazil) and Sodium Carbonate (purity 99.0%, Labimpex Indústria e Comércio de Produtos para Laboratório/Brazil). In the adsorption experiments, crystal

violet (Tris (4-(dimethylamino) phenyl) methylium chloride, purity 99.0%, Neon Reagentes Analíticos/Brazil) was used as an adsorbate solution.

2.2. Synthesis Ni/In-LDH

Ni/In-LDH was synthesized from $Ni(NO_3)_2.6H_2O$ (30 mmol, 8.7237g) and $In(NO_3)_3.5H_2O$ (10 mmol, 3.9090g) dissolved in 50 mL of deionized water. A solution of NaOH (2*M*) and Na_2CO_3 (0.2*M*) was added dropwise until *pH* 10 was reached. The mixture obtained was stirred at 80ºC (353.15 K) for 4 h, and the obtained solid was centrifuged, and washed with deionized water in abundance, until the filtrate reached neutral *pH*. Subsequently, the material was dried at 50ºC for 24 h [14].

2.3. Characterization

The as-synthesized adsorbent was characterized by the following methods: X-ray diffraction (XRD) method (Rigaku, Miniflex 300, Japan, with Cu Ka radiation filtered by Ni, λ = 1.54051 Å, 30 kV, 10 mA, 2θ = 5-100º) to verify the crystallinity of the synthesized adsorbent material; Fourier Transform Infrared Spectroscopy (FT-IR) method (Shimadzu, Prestige 21, Japan, amplitude of 400-4400 cm^{-1}) to evaluate the presence of functional groups; Scanning Electron Microscopy with Energy Dispersive Spectroscopy (SEM-EDS) method (TESCAN, Czech Republic, 10 kV acceleration and gold coating) to determine the presence of chemical elements and the homogeneity of the LDH material.; and Brunauer-Emmet-Teller (BET) method (New Win, Quantachrome, USA, N_2 adsorption isotherms at 77K) to determine the specific surface area.

2.4. Adsorption experiments

2.4.1. Determination of the point of zero charge (pH_{pzc}) and ideal pH for adsorption:

A sample containing 25 mg of the adsorbent was added to 50 mL of solution with a concentration of 50 mg L^{-1} of CV dye. The pH values ranged from 2 to 10, being adjusted with HCl (0.01 or 0.1M) and NaOH (0.01 or 0.1M), under constant agitation 140 rpm for 24 h at 25ºC (298.15 K). Then, the final *pH* of the solution was measured, and the solution was centrifuged for phase separation at 4000 rpm for 20 min. The experiment was performed in triplicate. During the adsorption experiments, the dye concentrations were determined by UV/Vis spectrophotometry (Shimadzu, UV-1280, Japan) at 581 nm. The adsorption capacities at equilibrium (q_e [mg g^{-1}]) were determined by Eq. (01) [10,12,17].

$$q_e = \frac{(C_0 - C_e).V}{W} \quad (01)$$

where C_0 and C_e are the initial and equilibrium concentrations [mg L^{-1}] of the solution, respectively, W is the mass of adsorbent [g] and V the volume of dye solution [L].

2.4.2. Adsorbent Dosage

The dosage of the adsorbent was evaluated in 50 mL of dye solution at a concentration of 50 mg L^{-1}. The dosages of adsorbent ranged from 10 to 2000 mg L^{-1}, at optimal *pH*, for a period of 24 h at 25°C (298.15 K). Subsequently, the solution was centrifuged and the adsorption capacities at equilibrium (q_e [mg g^{-1}]) were determined by Eq. (01) [17].

2.4.3. Kinetic studies

A sample of 12 mg of adsorbent was inserted in contact with 50 mL of CV dye solution (50 mg L^{-1}). The times ranged from 0 to 360 min under agitation at 25ºC (298.15

K) and ideal *pH*. The solution was centrifuged and the adsorption capacities at time *t* (q_t [mg g^{-1}]) were determined by Eq. (02) [18].

$$q_t = \frac{(C_0 - C_t).V}{W} \quad (02)$$

where C_0 and C_t are the initial and at a given time *t* concentrations of the dye solution, respectively [mg L^{-1}], W is the mass of adsorbent [g] and V the volume of dye solution [L].

Subsequently, the adjustments of mathematical models were performed from the kinetic data obtained. The pseudo-first order (PFO) model and the pseudo-second order (PSO) model were used, as expressed by Eqs. (03) and (04), respectively [19]:

$$q_t = q_f\left(1 - e^{-k_f.t}\right) \quad (03)$$

$$q_t = \frac{k_s.t.q_s^2}{(1+k_s.t.q_s)} \quad (04)$$

where q_f and q_s are the theoretical values for the adsorption capacity of PFO and PSO, respectively [mg g^{-1}]; k_f and k_s are the adsorption rate constants of PFO [min^{-1}] and PSO [g mg^{-1} min^{-1}], respectively; and t is the elapsed time [min].

The diffusion mechanisms of the adsorption process were also investigated from the kinetic model of intraparticle diffusion, according to Eq. (05) [20]:

$$q_t = k_i t^{1/2} + C \quad (05)$$

where, k_i is the constant of the intraparticle diffusion rate [mg g^{-1} $min^{-1/2}$] and C is the thickness of the boundary layer [mg g^{-1}], both values obtained from the construction of the graph of q_t as a function of $t^{1/2}$.

2.4.4. Equilibrium studies

A sample of 12 mg of adsorbent was added in contact with 50 mL of dye solution for concentrations ranging from 25 to 500 mg L^{-1} of dye. Solutions were adjusted to the ideal *pH*, under constant agitation of 140 rpm, for temperatures of 40, 50, and 60ºC (313.15, 323.15 and 333.5 K) for 4 h. Solutions were then centrifuged and the adsorption capacities (q_e [mg g^{-1}]) were determined by Eq. (01) [21].

The isotherms were adjusted using the Langmuir, Freundlich and Liu models, expressed respectively by the Eqs. (06), (07), and (08) [22,23,24]:

$$q_e = \frac{Q_{max}.K_L.C_e}{(1+K_L.C_e)} \quad (06)$$

$$q_e = K_F C_e^{1/n_F} \quad (07)$$

$$q_e = \frac{Q_{max}.(K_g.C_e)^{n_L}}{(1+(K_g.C_e)^{n_L})} \quad (08)$$

where Q_{max} is the maximum adsorption capacity of the model [mg g^{-1}]; K_L, K_F and K_g are the equilibrium constants of Langmuir [L mg^{-1}], Freundlich [mg g^{-1} (mg L^{-1})$^{-1/n}$] and Liu [L mg^{-1}], respectively; n_F and n_L are the exponents of Freundlich and Liu, respectively.

2.4.5. Thermodynamic studies

The determination of thermodynamic parameters makes it possible to identify factors such as spontaneity, viability, and organization between adsorbate and adsorbent during the adsorption process. Thus, the equations of Van't Hoff (Eq. 09) and Gibbs-Helmholtz (Eq. 10) were combined into Eq. (11), to obtain the standard values of the variations of Gibbs free energy ΔG^0 [kJ mol^{-1}], enthalpy ΔH^0 [kJ mol^{-1}] and entropy ΔS^0 [kJ mol^{-1} K^{-1}] [25].

$$\Delta G^0 = -RTln(K_e^0) \quad (09)$$

$$\Delta G^0 = \Delta H^0 - \Delta S^0 T \quad (10)$$

$$ln(K_e^0) = \frac{\Delta S^0}{R} - \frac{\Delta H^0}{RT} \quad (11)$$

where, R is the universal constant [*kJ mol^{-1} K^{-1}*], T is the temperature [*K*], and is the K_e^0 thermodynamic equilibrium constant [dimensionless].

2.4.6. Ionic strength study

In determining the ionic strength, a sample of 12 mg of adsorbent was added to solutions of sodium chloride (0 to 0.1 mol L^{-1}) and CV (50 mg L^{-1}, *pH* = 8.0) and stirred (140 rpm) for 4h at 30°C (303.15 K). Subsequently, the solutions were centrifuged and the adsorption capacities at equilibrium (q_e [mg g^{-1}]) were determined by Eq. (01) [12]. All previous experiments were performed in triplicates.

2.4.7. Regeneration studies

An adsorbent mass ratio of 0.24 g L^{-1} was dispersed in a CV dye solution (50 mg L^{-1}, 140 rpm for 4 h at 30ºC (303.15 K)). The analytical standard ethanol (AS) was used as eluent and added in a volume of 50 mL for desorption for 1 h. The solution was centrifuged, and the retained material was washed with deionized water, separated, and reused in a new adsorption procedure maintaining the ratio of (S/L) of cycle 0 (0.24 g L^{-1}). Starting Cycle 0 was performed with 10 replicates, and final Cycle 3 was performed with 5 replicates due to adsorbent loss during recipient transference, while maintaining the adsorbent mass ratio. The dye concentration was determined by spectrophotometry in the UV/Vis region at a wavelength of 581 nm. The equilibrium adsorption capacity (q_e [mg g^{-1}]), was determined by Eq. (01) [10].

3. Results and discussion

3.1. Material characterization

A specific surface area of 106.07 m^2 g^{-1} was determined for Ni/In-LDH adsorbent material by BET analysis which was consistent with literature values for other LDH, such as 102.00 m^2 g^{-1} for CuMgAl [18] and Zn-Co and 116.40 m^2 g^{-1} [26]. However, this was lower than the literature values for biochar (136 m^2 g^{-1}) [13]. BET analysis also resulted a pore volume of 0.3823 cm^3 g^{-1} and an average pore size of 14.25 nm for Ni/In-LDH, indicating that CV molecules, with an approximately 0.972 nm of size, can readily penetrate the adsorbent pores, as well as access and bond to active sites [27].

XRD analysis pattern results presented the formation of crystal structures through the high-intensity reflections at the *2θ* angles of 5-100°, Fig. 2. Comparing with the pattern presented in Wang *et al.* [28] and for In_2O_3 and β-NiOOH obtained from Vieira *et al.* [29] and Narayan [30] studies, respectively, it is possible to affirm that there is the formation of *00l* basal reflections in lower values of *2θ*, identified with the Miller indices

of (003), (006) and (009) reflections, indicative of interlayer space between inorganic compounds and related to the periodicity of stacking along the *c* axis.

A large asymmetric basal reflection, (110), is presented with the increase of the angle 2θ, resulting from the turbostratic effects derived from the translational disorder of the layers of metal hydroxides along the axes *a* and *c*, removing the linear form of the reflections *hk0* [31].

Assuming a rhombohedral structure of hexagonal symmetry ($a = b$; $\gamma = 120°$), it is possible to calculate the network parameters *a* and *c* of the material, 0.219 and 2.349 nm respectively, and determine the basal spacing (BS) through the relation BS = c / 3 = 0.783 nm. This value is approximate to that found in the literature for Ni/In-LDH intercalated with CO_3^{2-}, 0.785 nm. The molecular size of CV being 0.972 nm is greater than the BS of the Ni/In LDH, therefore it cannot penetrate the interlayered sheets of Ni/In-LDH, leaving only the active sites at the surface of the porous adsorbent particles [27,28,32].

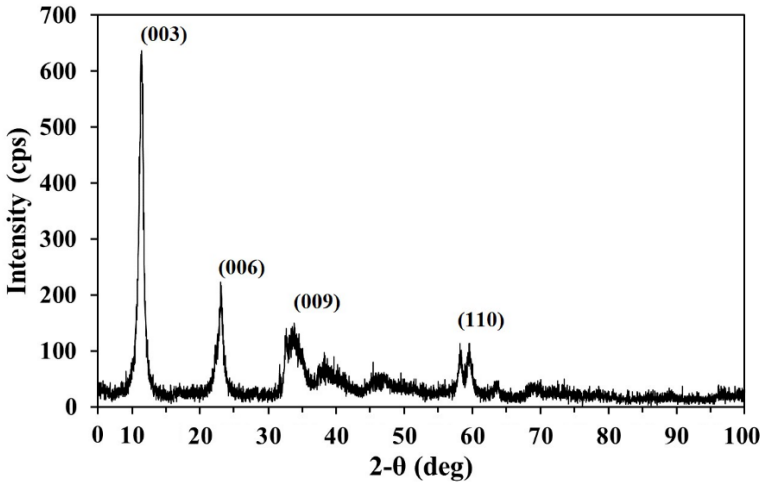

Figure 2 - XRD analysis of adsorbent Ni/In-LDH

FTIR analysis, Fig. 3.a), reveals an intense wide band around 3447 cm^{-1} that can be attributed to the *O-H* stretch of hydration water and hydroxyl groups of LDH. An apparent

shoulder at 3250 cm^{-1} to this broad band can be attributed to hydrogen bonding of CO_3^{2-} anions with interlayer H_2O [31].

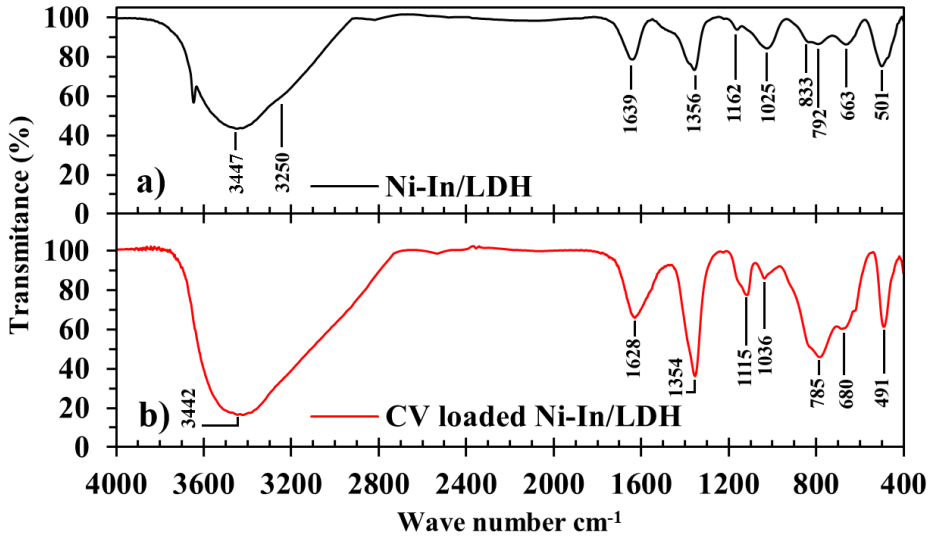

Figure 3 - FTIR analysis: a) adsorbent Ni/In-LDH, and b) CV loaded Ni-In/LDH.

A stretch at 1639 cm^{-1} reflects angular deformation δ_{HOH} of H_2O molecules, whilst that at 792 cm^{-1} can be attributed to the deformation of intermolecular H_2O. Intercalated CO_3^{2-} anions display moderate bands at 1356 and 1025 cm^{-1} due to C-O antisymmetric stretching ν_3, at 1162 cm^{-1} due to O-C-O asymmetric stretching and another stretch at 833 cm^{-1} for angular deformation of CO_3^{2-} anions [28,31,33].

Stretches at 663 cm^{-1} and 501 cm^{-1} may be attributed to *M-OH* stretch of both *Ni-OH* and *In-OH*. These results indicate the success in the synthesis process of Ni/In-LDH intercalated with CO_3^{2-} anions [34,35].

SEM-EDS analysis of the as-synthesized Ni/In-LDH presented the adsorbent material as irregular granules of varying sizes, Fig 4.a). EDS mapping verify a homogeneous distribution of the elements Ni and In (Fig. 4.b) and 4.c)) respectively [13]. This confirms that the production of Ni/In-LDH material can be achieved successfully.

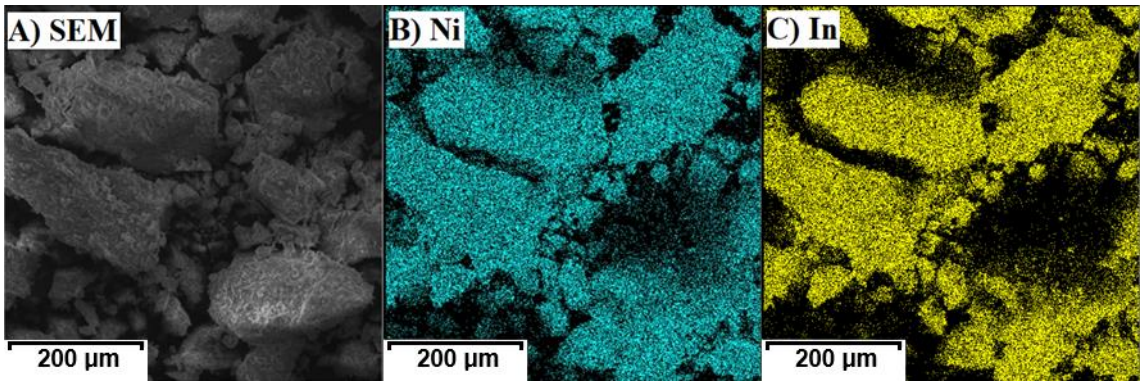

Figure 4 - SEM analysis with EDS mapping a) SEM, b) Ni, and c) In; magnification 200 times.

3.2. pH studies at point of zero charge (pH_{pzc}) and influence of pH

The influence of *pH* on the surface properties of the adsorbent and the degree of ionization of the adsorbate makes this parameter essential for the optimization of the adsorption process. The influence of the initial *pH* on the adsorption of CV in Ni/In-LDH was investigated with pH_0 between 2 and 10, Figure 5.a). Other adsorption parameters were kept constant: 50 mL solution volume, 50 mg L^{-1} adsorbate, CV concentration 50 mg L^{-1}, agitation 140 rpm, for 4 h at 25°C (298.15 K).

The highest adsorption capacity value of 68.39 mg g^{-1} was attained at pH 8.0. Analysis of Fig. 5.a) revealed a pH_{pzc} of 7.3 when the final *pH* is equal to the initial *pH* of the solution. In addition, the adsorption capacity increases considerably with the increase of the initial *pH* of the process until it reaches relative equilibrium when $pH_0 > pH_{pzc}$. This phenomenon is due to the *pH* of the solution controlling the magnitude of the electrostatic charges donated by the ionized molecules of the dye. The lower adsorption capacity at $pH_0 < pH_{pzc}$ is due to the positively charged adsorbent surface from an abundance of H^+ ions with consequent repulsion between the positively charged surface and cationic dye. However, when $pH_0 > pH_{pzc}$, the pH is higher and the adsorbent surface is negatively charged (abundance of OH^-) favoring electrostatic interaction with the

cationic dye CV thus resulting in increased adsorption capacity, q_e. Therefore, pH 8.0 was defined as ideal in performing subsequent studies, ensuring optimal adsorption capacity for the process, as $pH_f > pH_{pzc}$ [12,17].

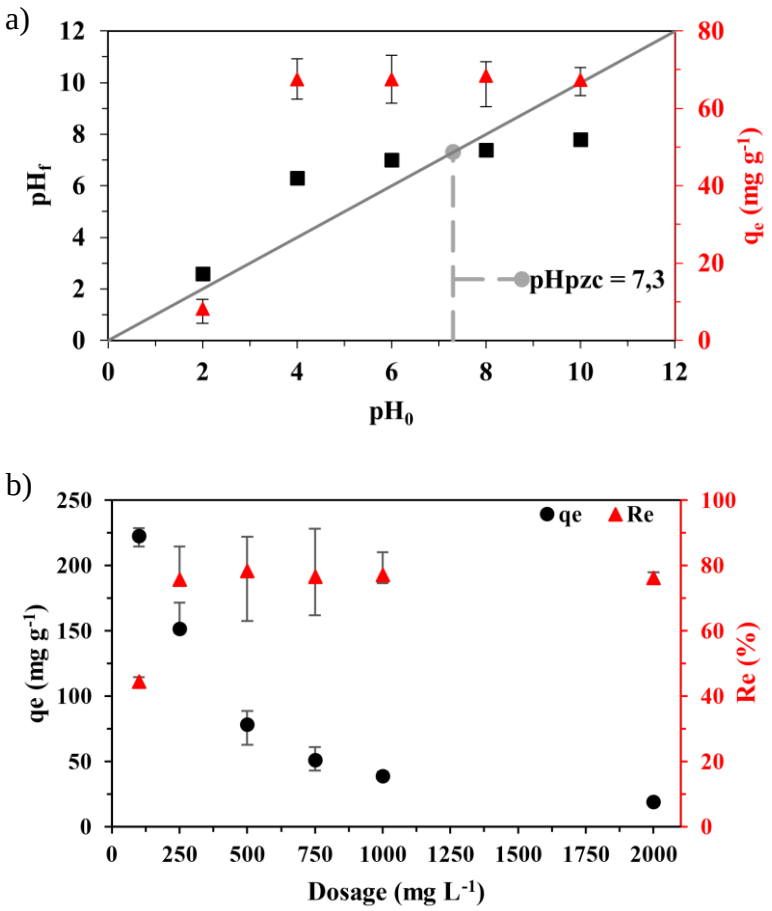

Figure 5 - a) pH_f as a function of pH_0 (black); adsorption capacity q_e [mg g^{-1}] (red); pH_{pzc}, (gray) (Experimental conditions: C_0 = 50 mg L^{-1} CV, 500 mg L^{-1} adsorbent, 140 rpm, 4 h, 25°C); b) Adsorption capacity q_e [mg g^{-1}] (black) as function of adsorbent dosage; percentual removal Re(%) (red) as function of adsorbent dosage (Experimental conditions: C_0 = 50 mg L^{-1} CV, *pH* 8.0, 140 rpm, 4 h, 25°C)

3.3. Adsorbent dosage

The adsorption capacity of CV on Ni/In-LDH was assessed by varying the dosage of adsorbent between 10 and 2000 mg L^{-1}, with the dye solution (50 mg L^{-1}, pH 8.0) at 140 rpm, for 4h at 25°C (298.15 K). CV removal (*Re%*) increases rapidly from 44.5 to 75.6%, in the range between 100 and 240 mg L^{-1}, Fig. 5.b). This is due to the increase in the contact surface between the adsorbent and adsorbate available, keeping in equilibrium at a dosage above 240 mg L^{-1} [17]. Therefore, the dosage established for the other experiments was 240 mg L^{-1}.

3.4. Kinetic studies

Adsorption kinetics are used to determine the efficiency of the adsorbent. The adsorption profile of CV in Ni/In-LDH was verified over a contact time ranging from 0 to 240 min (CV C_0 of 50 mg L^{-1}, *pH* 8.0, 140 rpm, at 25°C (298.15 K), adsorbent 240 mg L^{-1}), Fig. 6.a). The adsorption capacity reached equilibrium in 30 min of contact between adsorbate solution and adsorbent material with little change in adsorption capacity (*qt*) with any further increase in contact time *t*.

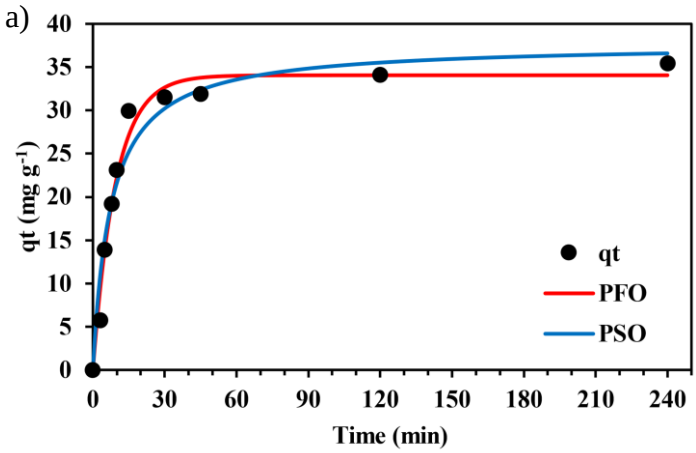

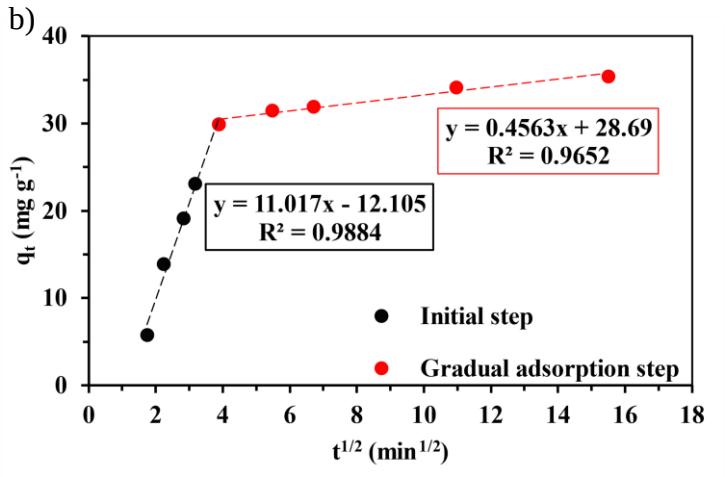

Figure 6: a) Kinetic curve for CV adsorption on Ni/In-LDH; b) Ni/In-LDH CV initial curve (black), intraparticle diffusion curve (red); (Experimental conditions: C_0 = 50 mg L^{-1}, pH = 8.0, 140 rpm, 25°C and adsorbent dosage 240 mg L^{-1})

The reaction models of PFO and PSO, Equations (03) and (04), were used to interpret the adsorption kinetics curve obtained experimentally. The obtained adsorption parameters for CV in Ni/In-LDH are presented in Table 1. Satisfactory adjustment was obtained for PFO due to higher value of the coefficient of determination (R^2) and adjusted coefficient of determination (R^2_{adj}). In addition, the PFO model presented a lower mean relative error (ARE), reduced Chi-square (χ^2_{red}), and sum of deviations (SD), compared to the PSO model, thus highlighting the greater suitability of the PFO kinetic model. As such, the rate-limiting step in this mechanism was determined to involve diffusion process where the reaction rate depends only on the concentration of the adsorbate [19,36].

Table 1 – PFO and PSO models parameters.

Model	$k_{f;s}$ (min^{-1})	q_e (mg g^{-1})	R^2	R^2_{adj}	ARE (%)	χ^2_{red}	SD
PFO	1.06 x10^{-1}	34.06	0.9667	0.9619	4.04	4.65	2.16
PSO	3.56 x10^{-3}	37.72	0.9317	0.9219	5.29	9.53	3.09

From the analysis of the mechanism of intraparticle diffusion of adsorption, it was possible to observe multilinear plots that indicates the presence of two distinct steps (Fig. 6.b). An initial step due to surface adsorption and rapid external diffusion (boundary layer diffusion), and a second linear portion representing the gradual adsorption step occurring from 15 minutes of contact onwards, where the intraparticle diffusion is controlled by the adsorption rate. From Eq. (05), the slope k_i of the second linear portion characterizes the parameter of the adsorption rate corresponding to intramolecular diffusion, 0.45 mg g^{-1} $min^{-1/2}$, and the interception on the function axis is proportional to the thickness of the limit layer C = 28.69 mg g^{-1}. Since $C \neq 0$, it is possible to assert that the intraparticle diffusion mechanism is not the only rate controlling step of adsorption kinetics. Therefore, boundary layer and intraparticle diffusion mechanisms occur simultaneously as the rate limiting steps of mass transfer process that controls adsorption [20,36,37].

3.5. Isothermal equilibrium studies

Adsorption equilibrium isotherms (Fig. 7) were obtained at temperatures of 40, 50, and 60 °C (313.15, 323.15 and 333.15 K), for increasing concentrations of CV (25 to 400 mg L^{-1}) whilst other experimental conditions were maintained constant (pH 8.0, adsorbent dosage 240 mg L^{-1}, 140 rpm). The isotherms presented S2 shape, as presented by Giles *et al.* [38], assuming a vertical orientation of molecules adsorbed on the surface, moderate intermolecular interaction in the adsorbate and strong competition for active sites between adsorbate and solvent.

The adsorption capacity at equilibrium (q_e) highly increased with the increase in the concentration of solute at equilibrium (C_e), Fig. 7. This indicates that there was no saturation of all adsorption sites within the experimental range and the great potential of CV adsorption in the Ni/In-LDH adsorbent [13].

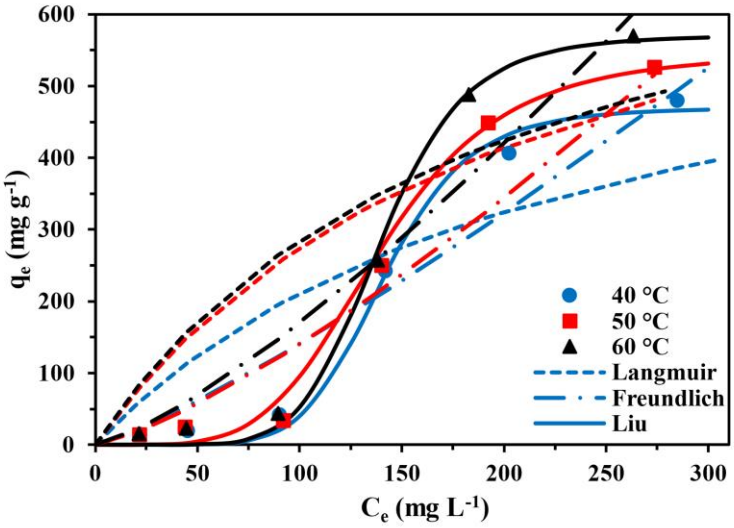

Figure 7 - Isothermal curves for adsorption of CB in Ni/In-LDH (Experimental conditions: dosage of adsorbent of 240 mg g^{-1}, pH 8,0, constant agitation of 140 rpm, for 4 h).

Three adsorption isotherm non-linear models of Langmuir (Eq. 06), Freundlich (Eq. 07), and Liu (Eq. 08) were tested for the isothermal equilibrium. Langmuir's [22] model considers the hypothesis of a monolayer adsorption process, leading to a maximum adsorption capacity (Q_{max}) as the energetically equivalent active sites present on the adsorbent's surface are filled. Freundlich [23] hypothesizes in his model that the adsorption process occurs infinitely and heterogeneously, assuming that the adsorbate concentration on the surface of the adsorbent increases exponentially as the initial concentration of the adsorbate increase, which leads to the formation of multilayers of adsorbate as the active sites on the surface of the adsorbent are filled and the adsorbate-adsorbate interactions create new energetically different active sites and the formation of a new adsorbate layer. Liu's [24] isotherm model combines Langmuir's and Freundlich's models by assuming the saturation of the energetically different active sites. Therefore,

Liu's model also discards the monolayer and infinite adsorption assumptions, respectively [19].

Table 2 contains the fitted models parameters obtained, where Liu's model presented good values of $R^2 > 0.9502$ and $R^2adj > 0.9412$ fits for all isotherms models analyzed, as well as lower values of ARE < 57.56%, $\chi^2red < 2064.35$ and SD < 45.44, compared to the Langmuir's and Freundlich's model fits. Liu's model correlation with the experimental data, indicated the presence of preferential active adsorption sites energetically different and their saturation. This allowed to reject the hypotheses of monolayer adsorption of the Langmuir model and infinite adsorption of the Freundlich model.

Table 2 – Isothermal parameters of Ni/In-LDH adjusted by Langmuir, Freundlich and Liu models.

	Temperature (°C)		
Model	40	50	60
Langmuir			
K_L (L mg^{-1})	4.34 x10^{-3}	4.79 x10^{-3}	5.19 x10^{-3}
Q_{max} (mg g^{-1})	697.97	846.42	832.65
R^2	0.7126	0.7711	0.6726
R^2_{adj}	0.6974	0.7520	0.6399
ARE (%)	231.56	298.10	284.66
χ^2_{red}	11090.18	15537.09	20477.06
SD	105.31	124.65	143.10
Freundlich			
K_F (mg g^{-1} (mg L^{-1})$^{-1/n}$)	0.555	0.359	0.413
n_F	0.83	0.77	0.77
R^2	0.8480	0.8696	0.8614
R^2_{adj}	0.8400	0.8588	0.8475
ARE (%)	92.64	8480	87.22
χ^2_{red}	5863.93	8187.14	8671.69
SD	76.58	90.48	93.12
Liu			
K_g (L mg^{-1})	7.07 x10^{-3}	7.12 x10^{-3}	7.14 x10^{-3}
Q_{max} (mg g^{-1})	469.53	546.65	570.95
n_L	6.84	4.62	6.80

R^2	0.9715	0.9502	0.9646
R^2_{adj}	0.9683	0.9412	0.9568
ARE (%)	53.40	57.56	50.07
χ^2_{red}	1161.22	2064.35	2458.27
SD	34.08	45.44	49.58

412

413 Accordingly, the value of the Liu equilibrium constant parameter (K_g), that
414 represents the adsorbent-adsorbate affinity, tends to increase with the temperature
415 indicating that adsorption is favored at elevated temperatures. Similarly, providing the
416 greatest value for maximum adsorption capacity (Q_{max}) of 570.95 mg g^{-1} at 60°C for the
417 study, due to the driving force gradient that increases with the adsorbate concentration
418 [39].

419 Table 3 compares the Q_{max} and *Re*(%) value in this study for the adsorption of CV
420 in Ni/In-LDH adsorbent with other methodologies and adsorbents from the literature used
421 on the removal of CV. The higher adsorption capacity of the adsorbent Ni/In-LDH
422 indicates this material's greater efficiency and potential in the removal of CV dye in
423 aqueous solutions compared to adsorbent materials synthesized trough other
424 methodologies.

425

426 Table 3 – Comparison between the maximum adsorption capacity Q_{max} and Removal
427 efficiency *Re* (%) in several studies for CV

Adsorbent	Q_{max} (mg g^{-1})	*Re*(%)	Reference
Ni/In-LDH	570.95	78.33	This work
Almond Shell	12.20	83.00	[17]
Zn-Al LDH carbon coated	128.87	97.87	[11]
ZVI-GAM	172.41	-	[18]
Clay	231.74	-	[7]
Biochar novel / Mg/Al-LDH	364.70	-	[12]
CaAl/Biochar (H_3PO_4)	496.55	71.00	[13]

428

429 3.6. Thermodynamic studies

A Van't Hoff diagram (Fig 8.a)) was obtained from Eq. (10) where the value of the thermodynamic constant (K_e^0) was estimated from the parameters from the previous adjustment of the Liu model. The parameter K_g [L mg^{-1}] was used in Eq. (12) to obtain K_e^0 [dimensionless] [19,25].

$$K_e^0 = \frac{1000\, K_G\, MM\, [adsorbate]^o}{\gamma} \quad (12)$$

where, MM is the molar mass of the adsorbate [g mol^{-1}]; [adsorbate]° is the standard concentration of the adsorbate (is by definition 1 mol L^{-1}); γ is the activity coefficient of the adsorbate and a unitary value is assumed for dilute solutions [dimensionless] [25].

a)

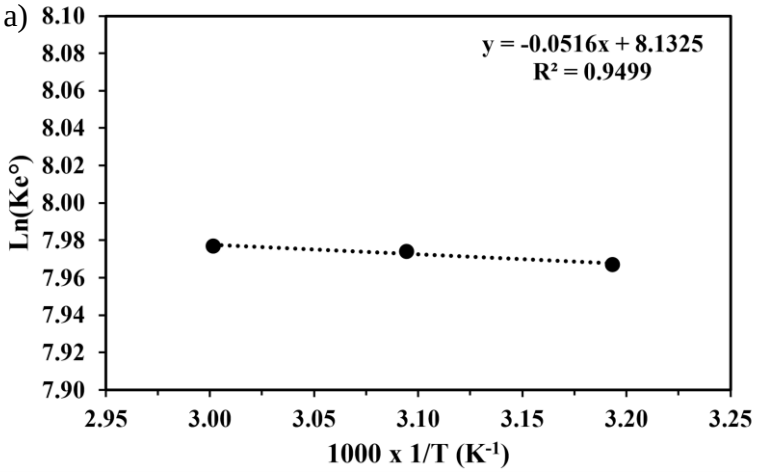

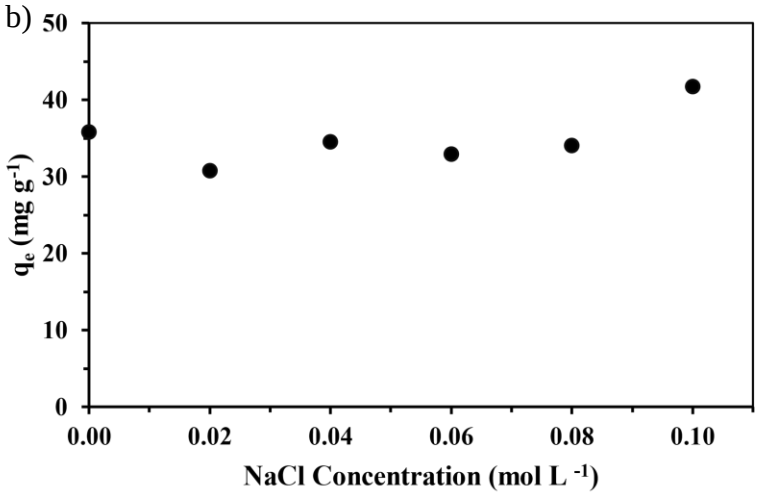

Figure 8 - a) Van't Hoff diagram for obtaining the thermodynamic parameters of adsorption; b) Effect of ionic strength on CV adsorption capacity in Ni/In-LDH (Experimental conditions: C_0 = 50 mg L^{-1} CV concentration, 30ºC, adsorbent dosage of 240 mg g^{-1}, *pH* 8.0 and constant rotation of 140 rpm).

441

442 The thermodynamic parameters $\Delta G°$, $\Delta H°$ and $\Delta S°$ were calculated from the Van't
443 Hoff diagram (Fig. 8.a)) and Equations (10) and (11). The $\Delta H°$ and $\Delta S°$ values obtained
444 were 0.429 kJ mol^{-1} and 67.61 J mol^{-1} K^{-1}, respectively, whilst the $\Delta G°$ value for
445 temperatures 40, 50, and 60°C, were determined as -20.74, -21.42, and -22.10 kJ mol^{-1},
446 respectively.

447 The negative $\Delta G°$ values indicates that the adsorption of CV in Ni/In-LDH
448 adsorbent is spontaneous and favorable. In addition, the decreasing value of $\Delta G°$ with
449 increasing temperature suggests that the process is most favored at 60°C. The positive
450 value of $\Delta H°$, implies that the adsorption process is endothermic and physisorption
451 occurs, since $\Delta H° < 20$ kJ mol^{-1}. The positive value of $\Delta S°$ reflects the occurrence of
452 rearrangements at the solid-liquid interface and increased randomness during the
453 adsorption process [12,13,18].

454

3.7. Ionic strength study

Industrial liquid effluent and polluted groundwater generally have high concentrations of salts which can affect the CV adsorption process. Therefore, the influence of the ionic strength of salts on the removal of CV in Ni/In-LDH adsorbent was modeled using NaCl ranging from 0 to 0.1 mol L^{-1} [12,40]. Analysis (Fig. 8.b) revealed relatively constant q_e values with increasing NaCl concentrations but with moderate increase for the 0.10 mol L^{-1} solution. This behavior could be considered an indicative of a positive effect of the NaCl in the dissociation of dye molecules by facilitating the protonation of CV and consequently increasing electrostatic interactions between CV cations and the deprotonated surface of Ni/In-LDH. This lends further support that, Ni/In-LDH could technically be a viable adsorbent for the adsorption of CV present in industrial effluents and groundwater [12,41].

3.8. Regeneration studies

The desorption process makes it possible to reduce operating costs with adsorbent, being fundamental to evaluate the reuse of the material. From the value of q_e obtained in regeneration cycles 1, 2, and 3, it was possible to compare the percentual relation of each cycle to the adsorption capacity of CV in cycle 0, resulting in 70.78%, 75.59%, and 71.42%, respectively. The q_e in the successive cycles of regeneration of Ni/In-LDH adsorbent in alcohol is maintained between 70 and 75% of the adsorption capacity of cycle 0. Thus, the results presented in the study reveals that the Ni/In-LDH adsorbent could be recycled and reused in CV adsorption procedures for textile wastewater treatment. Additionally, Ni/In-LDH can be synthesized from precursor materials such as Nickel recovered from spent batteries and Indium obtained in LCD screens from discarded cellphones, thus lowering even further the costs of adsorption effluent

480 treatment. Therefore, Ni/In-LDH figures as a promising cost-effective adsorbent to
481 wastewater effluent treatment processes worldwide.
482
483 3.9. Interaction mechanisms of adsorption
484 An interaction adsorption mechanism can be suggested by considering the results
485 of the adsorbent's characterization, speciation, and standard enthalpy change's magnitude
486 [42]. The interaction mechanisms of adsorption were suggested in this study as follows,
487 Fig. 9.
488
489 3.9.1. Electrostatic attraction
490 Electrostatic attraction will happen if an adsorbent particle and the adsorbate
491 particle possess opposite charges [11,43]. As discussed in section 3.2., the removal of CV
492 from water was favored by when the solution pH was higher than the pH_{pzc}, indicating
493 the occurrence of electrostatic attraction between the negatively charged adsorbent
494 surface and the nitrogen atom of cationic dye CV, as described in Fig. 9.d).
495

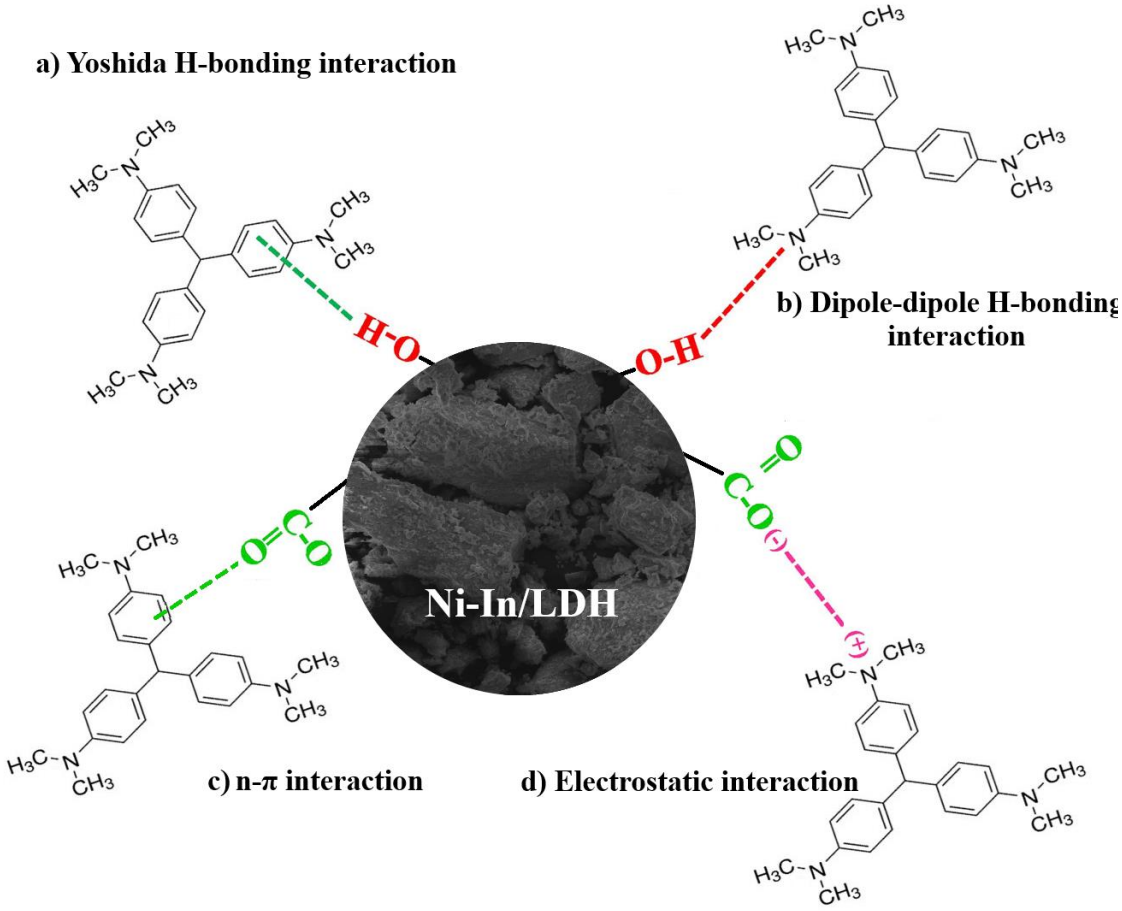

Figure 9 – Interaction mechanisms of adsorption

3.9.2. Hydrogen bond interactions

H-bonding interactions may occur with the presence of some functional groups such as -OH, -COOH, and -NH_2 acting as H-donor to H-acceptor molecules [44]. Two categories of H-bonding interactions could happen, dipole-dipole interactions between hydroxyl groups on Ni-In/LDH surface and nitrogen atoms in CV molecules, or Yoshida bonding, between the H-donor adsorbent surface and the aromatic groups of CV [45]. Analyzing the FTIR spectra obtained for the adsorbent Ni-In/LDH before and after adsorption of CV, Fig. 3.a and 3.b, respectively, it is possible to observe an intensity increase and a minor transition to lower wavenumber from 3447 to 3442 cm^{-1} after the

adsorption process may represent the occurrence of both Yoshida and hydrogen bonding, Fig. 9.a) and 9.b), respectively [43,46].

3.9.3. n-π interactions

n-π interactions as suggested by Mattson *et al.* [47] may occur when aromatic rings, such as those present in CV (Fig. 1), turn as electron acceptors meanwhile oxygen groups on the Ni-In/LDH adsorbent surface function as electron donors. The FTIR spectra results, Fig. 3, presents a decrease in intensity in the C-O stretch and a minor transition wavenumber from 1025 to 1036 cm^{-1}. Also, an increase in intensity and transition in wavenumber for the stretches related to CO_3^{2-} anions (C=O and O-C-O) from 1356 and 1162 cm^{-1} to 1354 and 1115 cm^{-1}. Stretches at 833 and 792 cm^{-1} merged into a more intense stretch at 785 cm^{-1} after adsorption of CV, meanwhile the stretch at 1639 cm^{-1} increased in intensity and had a minor transition in wavenumber to 1628 cm^{-1}, indicating that an interaction between the aromatic rings of CV and the electron donor surface of Ni-In/LDH might have occurred. This highly suggests that n-π interactions happened in the adsorption process, Fig. 9.c) [44,46].

4. Conclusions

In this work, the main objective was to investigate the adsorption capacity of Crystal violet dye in Ni-In/LDH adsorbent in different conditions. The adsorbent Ni/In-LDH intercalated with CO_3^{2-} was successfully synthesized and characterized. The adsorbent had a rhombohedral structure of hexagonal symmetry, and good homogeneity, with basal spacing (*BS*) of 0.783 nm and specific surface area of 106.07 m^2 g^{-1}. The optimal conditions of adsorption operation were pH 8.0, adsorbent dosage of 250 mg L^{-1}, temperature of 60°C, and potential for use of Ni/In-LDH in processes with high ionic

strength. The material presented a high value of maximum Q_{max} adsorption capacity in this study of 570.95 mg g^{-1}, contact time up to equilibrium of 30 min and maintained between 70% and 75% of the adsorption capacity in successive regeneration cycles. Kinetic studies indicated that the adsorption process followed the Pseudo first order (PFO) model. The isothermal study data best fitted the Liu isothermal model with R^2>0.9502, indicating the presence of multilayers and adsorption sites with different activation and saturation energies occupied by the adsorbate molecules. Thermodynamic studies indicated a spontaneous and endothermic adsorption process, and the mechanism of physisorption of CV in Ni/In-LDH. Interaction mechanisms of adsorption were proposed for the Ni-In/LDH and CV interactions, such as electrostatic, hydrogen, Yoshida, and n-π interaction bonds. The adsorbent Ni/In-LDH displayed excellent applicability in the removal of CV dye from aqueous solutions compared to other high performing adsorbents in the literature, demonstrating that Ni-In/LDH is a highly efficient adsorbent and a promising material to the effluent treatment industry.

Acknowledgments

The authors would like to thank FAPERGS (Foundation for Research Support of the State of Rio Grande do Sul), CNPq (National Council of Scientific and Technological Development), CAPES (Brazilian Agency for Improvement of Graduate Personnel), and SDECT (Department of Economic Development, Science and Technology of the State of Rio Grande do Sul) for financial support.

CRediT authorship contribution statement

Eduardo Teixeira Santos: Formal analysis; Investigation; Methodology; Writing - original draft. **Nicholas P. Power:** Writing - review & editing. **Satheesh**

Krishnamurthy: Writing - review & editing. **Daniel A. Bertuol:** Supervision; Writing - review & editing. **Eduardo H. Tanabe:** Conceptualization; Funding acquisition; Supervision; Writing - review & editing.

Declaration of Competing Interest

The authors declare that they have no known competing financial interests or personal relationships that could have appeared to influence the work reported in this paper.

Data availability

The data that has been used is confidential.

References

[1] United Nations, The United Nations World Water Development Report 2023: Partnerships Cooperation for Water, UNESCO, Paris, 2023.

[2] N. Pensupa, S. Leu, Y. Hu, C. Du, H. Liu, H. Jing, H. Wang, C.S.K. Lin, 2017. Recent Trends in Sustainable Textile Waste Recycling Methods: Current Situation and Future Prospects. Top Curr. Chem., 375, 76. https://doi.org/10.1007/s41061-017-0165-0

[3] H.M. Solayman, Md.A. Hossen, A.A. Aziz, N.Y. Yahya, K.H. Leong, L.C. Sim, M.U. Monir, K. Zoh, 2023. Performance evaluation of dye wastewater treatment technologies: A review. J. Eviron. Chem. Eng., 11, 109610. https://doi.org/10.1016/j.jece.2023.109610

[4] L. Meili, P.V.S. Lins, M.T. Costa, R.L. Almeida, A.K.S. Abud, J.I. Soletti, G.L. Dotto, E.H. Tanabe, L. Sellaoui, S.H.V. Carvalho, A. Erto, Adsorption of methylene blue on agroindustrial wastes: Experimental investigation and phenomenological modelling, Prog. in Biophys. Mol. Biol., 141 (2019) 60 - 71. https://doi.org/10.1016/j.clay.2018.10.012

[5] E. Rápó, S. Tonk, 2021. Factors Affecting Synthetic Dye Adsorption; Desorption Studies: A Review of Results from the Last Five Years (2017-2021). Mol., 26, 5419. https://doi.org/10.3390/molecules26175419

[6] S. Mani, R.N. Bharagava, R. N., Exposure to Crystal Violet, Its Toxic, Genotoxic and Carcinogenic Effects on Environment and Its Degradation and Detoxification for Environmental Safety. Rev. Environ. Contam. Toxicol., 237 (2016) 71–104. https://doi.org/10.1007/978-3-319-23573-8_4

[7] S. Bentahar, A. Dbik, M.E. Khomri, N.E. Messaoudi, A. Lacherai, Adsorption of methylene blue, crystal violet and congo red from binary and ternary systems with natural clay: Kinetic, isotherm and thermodynamic, J. of Environ. Chem. Eng., 5 (2017) 5921-5932. https://doi.org/10.1016/j.jece.2017.11.003

[8] M.W. Vasconcelos, S. Gonçalves, E.C. de Oliveira, S. Rubert, N. de C. Ghisi, 2022. Textile effluent toxicity trend: A scientometric review. J. Clean. Prod., 366, 132756. https://doi.org/10.1016/j.jclepro.2022.132756

[9] Z. Wang, M. Xue, K. Huang, Z. Liu,, Textile Dyeing Wastewater Treatment, In Houser, P. J. (Ed.), Advances in Treating Textile Effluent, InTechOpen, London, 2011, PP. 91 - 116. https://doi.org/10.5772/22670

[10] S. Razani, A.D. Tehrani, Development of new organic-inorganic, hybrid bionanocomposite from celulose nanowhisker and Mg/Al-CO3-LDH for Enhanced dye removal, Int. J. Biol. Macromol., 133 (2019) 892 - 901. https://doi.org/10.1016/j.ijbiomac.2019.04.149

[11] G. George, M.P. Saravanakumar, Facile synthesis of carbon-coated layered double hydroxide and its comparative characterisation with Zn-Al LDH: Application on Crystal violet and malachite green dye adsorption-isotherm, kinetics and Box-Behneken design, Environ. Sci. Pollut. Res., 25 (2018) 30236 - 30254. https://doi.org/10.1007/s11356-018-3001-3

[12] X. Tan, Y. Liu, Y. Gu, S. Liu, G. Zeng, X. Cai, X. Hu, H. Wang, S. Liu, L. Jiang, Biochar pyrolized from MgAl-layered double hydroxides pre-coated ramie biomass (Boehmeria nivea (L.) - Characterization and application for crystal violet removal, J. Environ. Manag., 184 Part 1 (2016) 85 - 93. http://dx.doi.org/10.1016/j.jenvman.2016.08.070

[13] J. Missau, D. Bertuol, E.H. Tanabe, 2021. Highly efficient adsorbent for removal of Crystal Violet Dye from Aqueous Solution by CaAl/LDH supported on Biochar. Appl. Clay Sci., 214, 106297. https://doi.org/10.1016/j.clay.2021.106297

[14] Y. Wang, Y. Zhou, T. Zhang, M. He, X. Bu, Two-dimensional ultrathin nanosheets of Ni-In-layered double hydroxides prepared in water: enhanced performance for DNA adsorption. RSC Adv., 4 (2014) 29968 - 29974. https://doi.org/10.1039/c3ra47728b

[15] R.F. Pinheiro, L. Michielin, T.R. Martins, T. Wildgrube, E.H. Tanabe, D.A. Bertuol, Application of mechanical processing operations for the recycling of nickel metal hydride batteries. J. Mat. Cycles Waste Manag., 23 (2021) 2148 - 2161. https://doi.org/10.1007/s10163-021-01280-x

[16] A.V.M. Silveira, M.S. Fuchs, D.K. Pinheiro, E.H. Tanabe, D.A. Bertuol, Recovery of indium from LCD screens of discarded cell phones. Waste Manage., 45 (2015) 334 - 342. https://doi.org/10.1016/j.wasman.2015.04.007

[17] I. Loulidi, F. Boukhilifi, M. Ouchabi, A. Amar, M. Jabri, A. Kali, S. Chraibi, C. Hadey, F. Aziz, 2020. Adsorption of Crystal Violet onto an Agricultural Waste Residue: Kinetics, Isotherm, Thermodynamics, and Mechanism of Adsorption. The Sci. World J., 1, 5873521. https://doi.org/10.1155/2020/5873521

[18] J. Liu, Y. Wang, Y. Fang, T. Mwamulina, S. Song, C. Peng, Removal of Crystal violet and methylene blue from aqueous solutions using the fly ash-based adsorbent material-supported zero-valent iron. J. Mol. Liq., 250 (018) 468 - 476. https://doi.org/10.1016/j.molliq.2017.12.003

[19] É.C. Lima, M.A. Adebayo, F.M. Machado, Kinect and Equilibrium Models of Adsorption, In: C. B., F. M., (Eds) Carbon Nanomaterials as Adsorbents for

654 Environmental and Biological Applications, Carbon Nanostructures Springer, Cham.,
655 2015, pp. 33-69. https://doi.org/10.1007/978-3-319-18875-1_3
656
657 [20] D. Bharali, R.C. Deka, Preferential adsorption of various anionic and cationic dyes
658 from aqueous solution over ternary CuMgAl layered double hydroxide, Coll. Surfa. A.,
659 525 (2017) 64 - 76. https://doi.org/10.1016/j.colsurfa.2017.04.060
660
661 [21] L. Deng, H. Zeng, Z. Shi, W. Zhang, J. Luo, Sodium dodecyl sulfate intercalated and
662 acrylamide anchored layered double hydroxides: A multifunctional adsorbent for highly
663 efficient removal of Congo Red, J. Coll. Interf. Sci., 521 (2018) 172-187.
664 https://doi.org/10.1016/j.jcis.2018.03.040
665
666 [22] I. Langmuir, The adsorption of gases on plane surfaces of glass, mica and platinum,
667 J. Am. Chem. Soc., 40, 9 (1918) 1361 - 1403. https://doi.org/10.1021/ja02242a004
668
669 [23] H. Freundlich, Adsorption in solution, Phys. Chem. Soc., 40 (1906) 1361-1368.
670
671 [24] Y. Liu, H. Xu, S.-F. Yang, J.-H. Tay, A general model for biosorption of Cd2+, Cu2+
672 and Zn2+ by aerobic granules, J. Biotechnol., 102 (2003) 233 - 239.
673 https://doi.org/10.1016/S0168-1656(03)00030-0
674
675 [25] É.C. Lima, A. Hosseini-Bandegharaei, J.C. Moreno-Piraján, I. Anastapoulos, A
676 critical review of the estimation of the thermodynamic parameters on adsorption
677 equilibria. Wrong use of equilibrium constant in the Van't Hoof equation for calculation

of thermodynamic parameters of adsorption, J. Mol. Liq., 273 (2019) 425 - 434. https://doi.org/10.1016/j.molliq.2018.10.048

[26] C. Qiao, Y. Zhang, Y. Zhu, C. Cao, X. Bao, J. Xu, One-step synthesis of zinc-cobalt layered double hydroxide (Zn-Co-LDH) nanosheets for high-efficiency oxygen evolution reaction, J. Mater. Chem. A, 3 (2015) 6878 - 6883. https://doi.org/10.1039/c4ta06634k

[27] M. Sarabadan, H. Bashiri, S.M. Mousavi, Removal of crystal violet dye by an efficient and low-cost adsorbent: Modeling, kinetic, equilibrium and thermodynamic studies, Korean J. Chem. Eng., 36 (2019) 1575 - 1586. https://doi.org/10.1007/s11814-019-0356-1

[28] Y. Wang, Y. Zhou, T. Zhang, M. He, X. Bu, X. Yang, Acetate-intercalated Ni-In layered double hydroxides with low infrared emissivity: Synthesis, delamination and restacked to form multilayer, Appl. Surf. Sci., 288 (2014) 710 - 717. https://doi.org/10.1016/j.apsusc.2013.10.109

[29] N.C.S. Vieira, E.G.R. Fernandes, A.A.A. de Queiroz, F.E.G. Guimarães, V. Zucolotto, Indium Tin Oxide Synthesized by a Low Cost Route as SEGFET pH Sensor. Mat. Res., 16 (2013) 1156 - 1160. https://doi.org/10.1590/S1516-14392013005000101

[30] R.T. Narayan, 2015. Effect of Crystallinity of β- and βbc-Nickel Hydroxide Samples on Chemical Cycling. Hindawi Publ. Corp., 1, 820193. https://doi.org/10.1155/2015/820193

[31] A.S. Prakash, P.V. Kamath, M.S. Hedge, Synthesis and characterization of the layered double hydroxides of Mg with Cr., Mater. Res. Bull., 35 (2000) 2189 - 2197. https://doi.org/10.1016/S0025-5408(00)00419-0

[32] W.H. Zhang, X.D. Guo, J. He, Z.Y. Qian, 2008, Preparation of Ni(II)/Ti(IV) layered double hydroxide at high supersaturation, J. of Eur. Ceram. Soc., 28 (2008) 1623-1629. https://doi.org/10.1016/j.jeurceramsoc.2007.11.016

[33] M.C. Portillo, O.P. Moreno, R.G. Pérez, R.P.Merino, H.S. Juarez, S.T. Cuapa, E.R. Rosas, Characterization and growth of doped-PbS in situ with Bi^{3+}, Cd^{2+} and Er^{3+} ions by chemical bath, Mat. Sci. Semicond. Proc., 72 (2017) 22 – 31 https://doi.org/10.1016/j.mssp.2017.09.012

[34] F. Chu, Z. Xu, Y. Zhou, S. Zhang, X. Mu, J. Wang, W. Hu, L. Song, 2021. Hierarchical core-shell TiO2@LDH@Ni(OH)2 architecture with regularly-oriented nanocatalyst shells: Towards improving the mechanical performance, flame retardancy and toxic smoke suppression of unsaturated polyester resin. Chem. Eng. J., 405, 126650. https://doi.org/10.1016/j.cej.2020.126650

[35] M.F. Hamza, A.A.M.A. El-Hamid, E. Guibal, A.A.H. Abdel-Rahman, R.E. Araby, 2023. Synthesis of a new pyrimidine-based sorbent for indium(III) removal from aqueous solutions – Application to ore leachate. Sep. and Purif. Technol., 314, 123514. https://doi.org/10.1016/j.seppur.2023.123514

[36] H.N. Tran, S.-J. You, A. Hosseni-Bandegharaei, H.-P Chao, Mistakes and inconsistencies regarding adsorption of contaminants from aqueous solutions: A critical review, Water Res., 120 (2017) 88-116. https://doi.org/10.1016/j.watres.2017.04.014

[37] G. Crini, H.N. Peindy, F. Gmbert, C. Robert, Removal of C.I. Basic Green 4 (Malachite Green) from aqueous solutions by adsorption using cyclodextrin-based adsorbent: Kinectic and equilibrium studies, Sep. Pur. Tech., 53 (2007) 97 - 110. https://doi.org/10.1016/j.seppur.2006.06.018

[38] C.H. Giles, T.H. Macewan, S.N. Nakhwa, D. Smith, Studies in adsorption. Part XI. A System of classification of adsorption isotherms, and its use in diagnosis of adsorption mechanisms and in measurement of specific surface areas of solids, J. Chem. Soc., 846 (1960), 3973-3993.

[39] A. Bonnila-Petriciolet, D.I. Mendoza-Castillo, G.L. Dotto, C.J. Duran-Valle, I.T. de Aguascalientes. Adsorption in Water Treatment, in: Ref. Modul. Chem., Mol. Sci. and Chem. Eng., Elsevier Inc. 2019. https://doi.org/10.1016/B978-0-12-409547-2.14390-2

[40] D.A. Yaseen, M. Scholz, Textile dye wastewater characteristics and constituents of synthetic effluents: a critical review, Int. J. of Environ. Sci. and Tech., 16 (2019) 1193 - 1226. https://doi.org/10.1007/s13762-018-2130-z

[41] Y. Wang, L. Zeng, X. Ren, H. Song, A. Wang, Removal of Methyl Violet from aqueous solutions using poly (acrylic acid-co-acrylamide)/attapulgite composite, J. Environ. Sci., 22 (2010) 7 - 14. https://doi.org/10.1016/S1001-0742(09)60068-1

[42] D.S.P. Franco, J. Georgin, C.G. Ramos, M.S. Netto, B. Lobo, G. Jimenez, E.C. Lima, F. Sher, 2023. Production of adsorbent for removal of propranolol hydrochloride: Use of residues from Bactris guineesis fruit palm with economically exploitable potential from the Colombian Caribbean. J. Mol. Liq., 38, 121677. https://doi.org/10.1016/j.molliq.2023.121677

[43] Y. Gao, K. Liu, R. Kang, J. Xia, G. Yu, S. Deng, A comparative study of rigid MOFs for the adsorption of pharmaceuticals: Kinetics, isotherms and mechanisms, J. Hazard. Mat., 359 (2018) 248 - 257. https://doi.org/10.1016/j.jhazmat.2018.07.054

[44] E.D. Cruz, J. Missau, S.R. Collinson, E.H. Tanabe, D.A. Bertuol, 2023. Efficient removal of congo red dye using activated lychee peel biochar supported Ca-Cr layered double hydroxide. Environ. Nanotechnol. Monit. Manag., 20, 100835. https://doi.org/10.1016/j.enmm.2023.100835

[45] H.N. Tran, Y.-F. Wang, S.-J. You, H.-P. Chao, Insights into the mechanism of cationic dye adsorption on activated charcoal: The importance of π-π interactions, Process Saf. Eviron. Prot., 107 (2017) 168-180. https://doi.org/10.1016/j.psep.2017.02.010

[46] S. Singh, S. Perween, A. Ranjam, 2021. Dramatic enhancement in adsorption of congo red dye in polymer-nanoparticle composite of polyaniline-zinc titanate. J. Environ. Chem. Eng., 9, 105149. https://doi.org/10.1016/j.jece.2021.105149

776 [47] J.S. Mattson, H.B. Mark, M.D. Malbin, W.J. Weber, J.C. Crittenden, Surface
777 Chemistry of Active Carbon: Specific Adsorption of Phenols, J. Colloid Interface Sci.,
778 31 (1969) 116-130. https://doi.org/10.1016/0021-9797(69)90089-7